Physica A 586 (2022) 126502

Contents lists available at ScienceDirect

Physica A

journal homepage: www.elsevier.com/locate/physa

Car-following characteristics and model of connected autonomous vehicles based on safe potential field

Yanfeng Jia, Dayi Qu *, Hui Song, Tao Wang, Zixu Zhao

School of Mechanical and Automotive Engineering, Qingdao University of Technology, Qingdao 266520, China

ARTICLE INFO

Article history:
Received 23 July 2021
Received in revised form 5 October 2021
Available online 12 October 2021

Keywords:
Required safe distance
Lennard-Jones
Safe potential field
Connected and autonomous vehicle
Car-following model

ABSTRACT

Aiming at the characteristics of connected and autonomous vehicle (CAV) which makes autonomous decision by perceiving the surrounding environment, a safe potential field model including lane marking potential field, road boundary potential field and vehicle potential field is established to describe the safe risk of CAV in the process of driving. In the process of building the safe potential field model, aiming at the defect that the existing vehicle potential field function has independent gravitational and repulsive expressions, a unified function of vehicle potential field based on Lennard-Jones potential is established by referring to the relationship of intermolecular interaction, and the parameter of vehicle's acceleration is considered into the vehicle potential field model. The statistical analysis of the parameter reveals that the change of acceleration directly affects the distribution of vehicle potential field and reflect the dynamic trend of vehicle's safe potential field under different driving states. Then, the safe potential field is applied to the car-following behavior of CAV, and the model's parameters are calibrated by Shanghai natural driving dataset; Finally, compared with the existing classic IDM and VTH models, the simulation results show that: the model still has smoother response curves in the three car-following scenarios designed to improve the safety and efficiency, which verifies the effectiveness of the model. The research results can lay a theoretical foundation for decision making behavior of safe driving, and also provide a unique way for the research of CAVs' safe technology.

1. Introduction

The research on car-following behavior has a long history. The existing car-following models can be divided into safe distance [1–3], physiological–psychological [4–6], stimulus–response [7–9] and artificial intelligence [10,11] from the perspective of traffic engineering. From the perspective of statistical physics, they can be divided into optimized speed [12–14], cellular automata [15,16] and intelligent driver [17]. The models are mostly constructed considering the kinematics and dynamics of vehicle and the driver's characteristics, such as driving style, reaction time, relative speed and distance, etc. Later, some scholars gradually applied the artificial potential field to the field of traffic and made some achievements. The concept of artificial potential field appeared at the end of the 20th century and it was first applied to the path planning of robots [18]. Inspired by this, Sattel et al. [19] extended the concept of robotic elastic bands to the motion planning of autonomous vehicle and proposed a planning algorithm based on potential field theory. Ni et al. [20] proved the objectivity and universality of artificial potential field in the traffic field from a macro and micro perspective, and

* Corresponding author.
E-mail address: dyqu@263.net (D.Y. Qu).

https://doi.org/10.1016/j.physa.2021.126502
0378-4371/

they used NGSIM data to calibrate the parameters of the car-following model. Hsu et al. [21] proposed a new gravity car-following model based on the concept of gravitational field, which describes the car-following behavior through a series of attractive and repulsive forces related to the vehicle and the space in front of it. Wolf et al. [22] also constructed the vehicle potential field into a wedge shape based on the artificial potential field theory, and they analyzed that vehicles at different speeds have different speed potentials as additional inputs in driver assistance equipment. Wang et al. [23] established a unified model of "vehicle safety field" of the closed-loop system by man–vehicle–road based on the research foundation of the predecessors and verified the model with real vehicles. It shows that the model can provide an effective method to assess driving risk for the complex traffic environment. Qu et al. [24] analyzed the molecular dynamics characteristics of vehicle's interaction and established a molecular car-following model through the potential function, and they verified that the model has high accuracy. Li et al. [25] proposed a simplified car-following model based on artificial potential field from the perspective of stimulus–response, but the factors considered in the model were relatively simple. Yang et al. [26] considered the influence of lateral distance on car-following behavior, and they expressed a single vehicle as a unit point charge in the electric field. The attractive potential energy and the repulsive potential energy simplifies the various influencing factors on the target vehicle in the actual car-following behavior. In this way, the factors affecting the traffic can be simplified to the mutual attraction and repulsion between the vehicles, so that the car-following behavior can be studied from a new perspective. However, with the emergence of connected and autonomous vehicles, the car-following characteristics need to be re-understood. Liu et al. [27] introduced potential field theory to model traffic factors such as road boundaries, lane markings, and vehicle driving. They used the overall potential function as a constraint and established a control method for the model predictive control problem. The simulation results show that the method can provide decision-making control basis for future autonomous vehicles in different traffic environments. Li et al. [28–30] proposed a novel methodology for risk perception and warning strategy based on safety potential field model to minimize driving risk in the CAVs environment. Then, they developed a driving risk potential field-based car-following model (DRPFM) to remedy the failure of acceleration consideration under the conventional environment. Later, they developed an alternative CAVs platoon dynamic control method based on the model predictive control (MPC) framework and safety potential field model. Some experiments were performed to verify the validity of their platoon control strategy. The Intelligent driver model (IDM) can complete the transformation between traditional car-following model and autonomous car-following model. Hua et al. [31] established a single-lane car-following model based on the Newell model, which considers vehicle-to-vehicle communication technology. Wu et al. [32] used the traditional longitudinal control model (LCM)) of vehicle based on the information of multiple preceding vehicles, and build a C-LCM model in an intelligent and connected environment, which can characterize the car-following characteristics of different vehicles. Path Laboratory of University of California, Berkeley has studied the car-following strategy of connected and autonomous vehicles for a long time, and verified it through small-scale real vehicles. However, at present, most of them focus on the car-following strategy in the time headway, while the research on other strategies is relatively small. Qin et al. [33] summarized such methods.

In summary, although there are many studies that apply the potential field theory to the field of traffic, they can only characterize the change of the potential field at a certain spatial position and current speed, few studies are carried out based on the intelligent and connected environment. Due to the lack of acceleration parameters, the distribution of the potential field cannot reflect the change in the movement trend of the vehicle. As for car-following in a intelligent and connected environment, scholars have conducted more research on the applicability of traditional car-following models on connected and autonomous vehicles. Therefore, this article considers that in an intelligent and connected environment, CAVs have the characteristics of recognizing lane lines and road boundaries by their own sensors, and obtaining the acceleration information of preceding vehicles in real time through the function of communication, and we construct a dynamic safe potential field model that includes the lane marking field, the road boundary potential field, and the vehicle potential field. Our innovations include: ① In order to make up for the defects that the previous vehicle potential field is independent, we first draw lessons from the interaction between molecules to establish a unified vehicle potential field function based on Lennard-Jones potential to more accurately describe the interactive behavior between vehicles. ② The acceleration is introduced into the safe potential field model and is applied to the car-following behavior of CAV and the change of acceleration directly affects the distribution of vehicle potential field and reflect the dynamic trend of vehicle's safe potential field under different driving states. ③ We use local data sets that are more in line with Chinese driving habits to calibrate parameters to improve the applicability of the model and this is less involved in the previous model.

The following content of this paper is divided into four parts: the second section is the concept and composition of the safe potential field. The third section is to establish a car-following model with safe potential field. The fourth section is to calibrate the parameters of the model based on the Shanghai Natural Driving Data Set and the genetic algorithm. In the fifth section, we choose to compare and evaluate with the classic IDM model and VTH model, and verify that our model can get better simulation effect. Finally, in the sixth section, we summarize the contribution of this paper.

2. The concept and composition of the safe potential field

2.1. The concept of potential field

From the perspective of physics, the field can be understood as an object with specific properties that will produce the force of interaction with other objects in a certain space around it without surface contact. The magnitude of the force

varies with the relative position of the objects. Because of the mutual force between objects, they have potential energy related to relative positions. Therefore, the potential field can be used to describe the ability of interaction in the entire space around the object. The potential field of an object is only related to its own properties and state. For example, if the property of an object is electric charge, and there will be an electric potential energy field around it, if the property of an object is a magnet, and there will be a magnetic potential energy field around it; and for mass, there will be a gravitational potential energy field around it.

2.2. The composition of the safe potential field

Similarly, there is a physical field similar to the above in the traffic system. The behavior that the vehicle is neither too close to nor far away from the preceding car can be regarded as the process that the vehicle constantly seeks the car-following equilibrium point by accelerating or decelerating under the force of the potential field of the car in front. Considering that in the intelligent and connected environment, CAV will be popularized in the future, and the driving rights of vehicles will be transferred from manual to autonomous decision-making. In addition to sensing other surrounding vehicles through sensors, CAV also perceives other traffic factors such as lane markings and road boundaries during driving. The safe driving of CAV can be regarded as the result of virtual resultant force of lane markings, road boundary and adjacent vehicles. Each factor that affects the vehicle can be regarded as a field source, and the safe potential field is the superposition of these field sources. Therefore, the safe potential field can be regarded as a physical field reflecting the impact of traffic factors on driving safety and it is composed of three parts in the simple traffic environment: the lane making potential field, the road boundary potential field and the vehicle potential field, which are represented by U_{L}, U_{R} and U_{V} respectively.

2.2.1. Lane marking potential field

We suppose that in a simple environment, there are two road markings, as shown in Fig. 1. One is black dotted line in the figure, and it is mainly used to separate vehicles traveling in the same direction. Vehicles are subject to certain constraints of this type of line during driving. The closer the vehicle is to the lane boundary, the greater its safe risk. However, when the vehicle changes lanes, the constraint, that is the value of potential field is also acceptable to the vehicle within the range of overcoming. The other is the double yellow line in the figure, which mainly separates vehicles traveling in different directions. Traffic laws stipulate that vehicles are not allowed to cross on a solid line, so the strength of the potential field formed by the cross-sectional position of the double yellow line is higher than the maximum strength of the black dotted line. The two types of lines jointly restrict the lateral motion of the vehicle, so that the vehicle can maintain the center of the lane as much as possible. Gunay et al. [34] shows that the position of the vehicle in the lateral direction within the lane is normally distributed, as shown in Fig. 2. This phenomenon can also be explained well from the perspective of the potential field. The position of the leftmost lane marking of the prescribed road is the origin of the x-axis. Therefore, we use the quasi-Gaussian function to represent the lane marking potential field distribution:

$$U_{\mathrm{L}} = \sum_{i=1}^{N-1} P_l \cdot \exp\left[-\frac{(x-x_i)^2}{2\delta^2}\right] \cdot \frac{x-x_i}{|x-x_i|} \tag{1}$$

where N is the number of lane lines in the cross section of the road; P_l is the intensity coefficient of different types of lane marking potential field, which is used to determine the maximum peak value of field strength of lane marking, P_1 is a white dashed line, P_2 is a double yellow line, and $P_1 \ll P_2$; x_i is the abscissa position of the ith line; δ is used to determine the ascending and descending speed of the lane marking potential field and is proportional to the width of the lane.

2.2.2. Road boundary potential field

Compared with other static potential fields, the potential field formed by the road boundary has a higher restraining effect on vehicles, and tends to infinity as the vehicles continue to approach. Its purpose is to seriously warn CAV to deviate from the normal driving direction, prevent vehicles from getting too close to reduce the risk of collision and even out of the road. This risk will not increase linearly as the vehicle approaches, but as the distance shortens, the safe risk will increase rapidly. The distribution of the road boundary field is shown by the blue dashed line in Fig. 3. Therefore, the form of the potential field of road boundary repulsive force is as follows:

$$U_{\mathrm{R}} = \sum_{r=1}^{2} \frac{1}{2}\lambda \left(\frac{1}{|x^r|}\right)^2 \cdot \frac{x^r}{|x^r|} \tag{2}$$

where r is the road boundary line, and we stipulate that $r = 1$ is the left boundary, and $r = 2$ is the right boundary. x^r is the distance from the vehicle to the road boundary r in the x-axis direction; λ is the gain parameter of position .

We set $P_1 = 2$, $P_2 = 8$, $\sigma = 1.22$, $\lambda = 3$ based on the paper [35]. According to Eqs. (1) and (2), the distribution of lane marking field and road boundary field can be drawn, as shown in Fig. 3, and the three-dimensional potential field formed by their superposition is shown in Fig. 4. It should be noted that the figure only contains the lane marking potential field and the road boundary potential field, and does not include vehicles and other traffic facilities or obstacles.

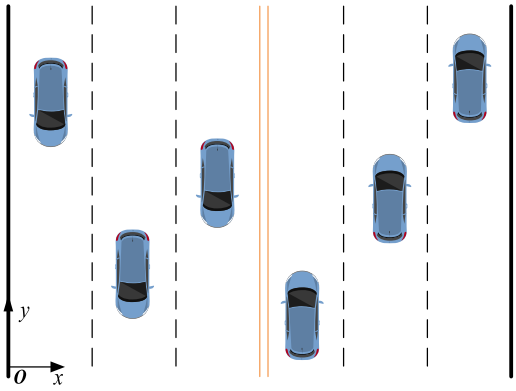

Fig. 1. Simplified environment of vehicle driving.

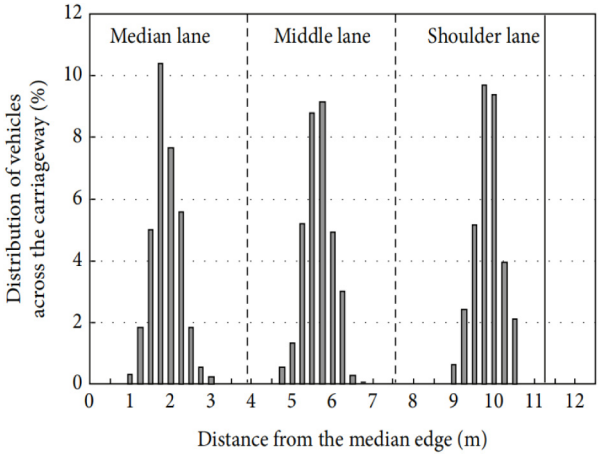

Fig. 2. Distribution of vehicles across the carriageway.

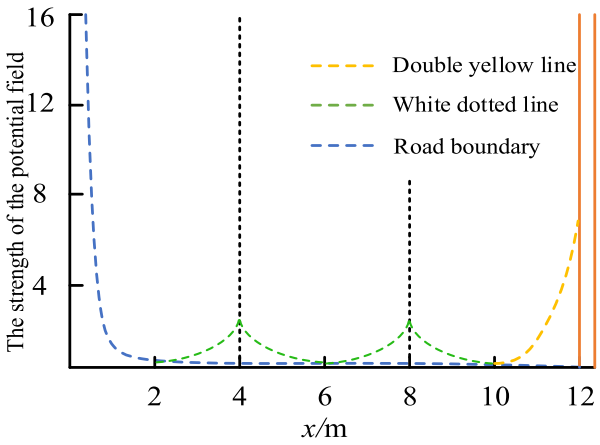

Fig. 3. Potential field distribution of Lane line and road boundary.

From the figure, we can see the contrast of the potential field intensity of different lane markings and road boundary. The intensity of the road boundary potential field is much larger than the lane marking potential field, and it decreases with the increase of the distance. The strength of the combined potential field reaches the peak at the location of the lane marking and the road boundary, and decreases to the minimum at the center of the lane along the *x*-axis. To ensure safety, the vehicle will make itself in the lower position of the potential field as much as possible to reduce safe risks.

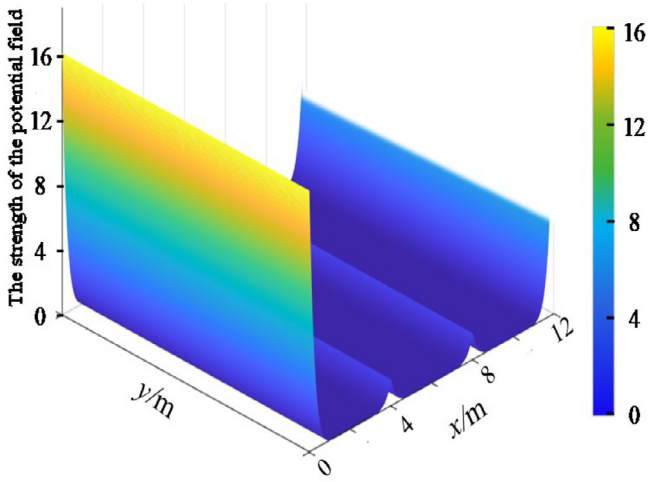

Fig. 4. Superlay diagram of various potential fields.

2.2.3. Vehicle potential field

The potential field of the vehicle comes from vehicles on the road. The paper [36] followed the idea of artificial potential field to study the car-following behavior of CAV. The artificial potential field includes the gravitational field and the repulsive field, which was originally used for robot path planning. The target generates gravitation on the object and guides the object toward it. The obstacle generates repulsion on the object to avoid collision. The specific acceleration expression generated by the short-range repulsive force is as follows:

$$a_s = -\rho M_{n+1} \frac{e^{-\beta_1 a_{n+1} + \alpha v_{n+1}}}{\tau \cdot \Delta x} \cdot e^{\beta_2 v_n} \tag{3}$$

where M_{n+1} is the equivalent mass of the n+1th vehicle; ρ, β_1 and β_2 are undetermined parameters; τ is the critical threshold of safety distance; α is the undetermined parameter related to speed; Δx is the inter-vehicle distance; a_{n+1} and v_{n+1} are the acceleration and speed of the n+1th vehicle, respectively.

The specific acceleration expression generated by the remote gravitational force is as follows:

$$a_r = a_{\max} \tanh\left[\delta\left(v_0^{(\alpha)} - v_n\right)\right] \tag{4}$$

where $a_{\max}$ is the maximum allowable acceleration of the vehicle; $v_0^{(\alpha)}$ is the desired speed of the vehicle; δ is the coefficient of the difference between the current speed and the desired speed of the vehicle.

However, the functions of gravitation and repulsion selected above are independent and separate and it is easy to cause excessive gravitation in the case of long distance. so it is particularly important to choose a uniform and appropriate function for vehicle potential field.

The vehicles on the road are miniaturized to molecules, and the position where the resultant force is zero between the molecules is called the equilibrium distance r_0, as shown in Fig. 5. There is also such a balanced distance in the process of car following, that is, the required safe distance of vehicle. When the distance between vehicles is less than the required safe distance, it will be subjected to the short-range repulsion of the preceding vehicle. When the actual distance is greater than the required safe distance, it will be subjected to the long-range gravitation of the preceding vehicle. Car-following behavior can be regarded as an operation to find a suitable safe distance and then accelerate or decelerate under the resultant force. The characteristics that the vehicles are neither far away from nor too close to the preceding vehicle are similar to the resultant motion of molecules, In reference [37], a car following model based on the Lennard-Jones potential is as follows:

$$\dot{v}_n = \eta_0 \left[2\frac{X_r^6}{L^7} - \frac{1}{L}\right]\left(\frac{X_r}{L}\right)^6 \tag{5}$$

where η_0 is a undetermined coefficient, X_r is the required safe distance, L is the actual distance between vehicles.

Yanakiev et al. [38] thought that the required safe distance of vehicles is not only related to the current vehicle's speed, but also related to the speed difference between the front and current vehicle. According to the established car-following strategy of VTH, the required safe distance is as follows:

$$X_r = (t_0 - c_v v_r)\, v_n \tag{6}$$

where v_n is the speed of the nth vehicle, t_0 and c_v are coefficients to be calibrated and greater than 0, v_r is the relative speed of the front and current vehicle.

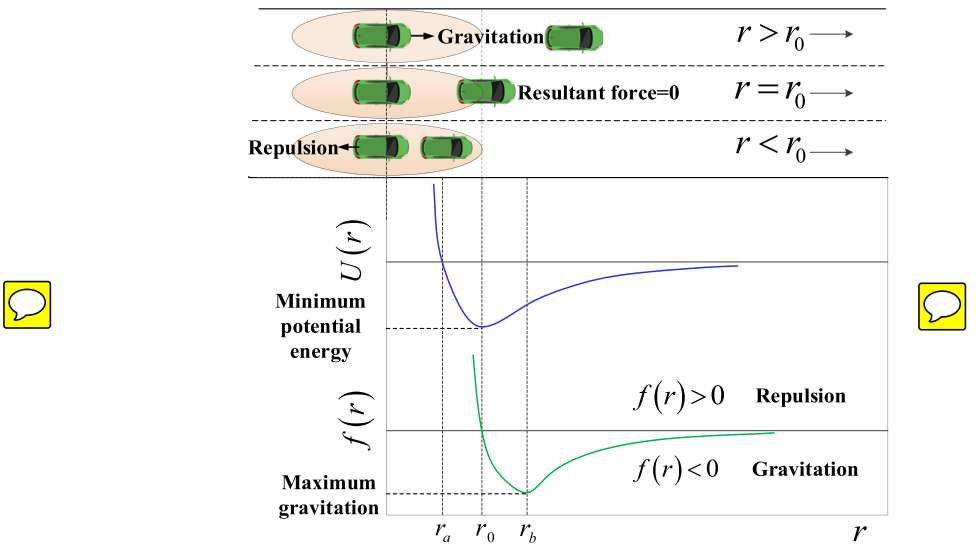

Fig. 5. Comparison between intermolecular interaction and car-following behavior.

The above car-following model is based on the function of Lennard-Jones 6–12 potential [39], which is widely used in molecular dynamics modeling, as follows:

$$U_{6,12}(r) = 4\varepsilon\left[(r_0/r)^{12} - (r_0/r)^6\right] \tag{7}$$

where ε is the energy scale, r_0 is the equilibrium distance between molecules, r is distance between molecules, $(r_0/r)^{12}$ is the repulsive term, that is, the short-range repulsion between molecules, $(r_0/r)^6$ is the gravitational term, that is, the long-range gravitation between molecules. When r is very large, the gravitation between molecules is close to zero.

It should be noted that when two vehicles are far away, it usually represents low traffic scenario, that is, free flow. At first, the vehicle may accelerate, but when it finally reaches the steady state, it is more likely to run at a constant speed at the maximum speed limit of the highway, even if the road in front is free. At this time, the acceleration of the vehicle is still close to zero.

In the Lennard-Jones potential model, the interacting force denoted by f of molecules in the potential field has the following relationship with the potential function:

$$f(r) = -\frac{\mathrm{d}U}{\mathrm{d}r} \tag{8}$$

From this we can calculate out:

$$f(r) = -24\varepsilon\left(2\frac{r_0^6}{r^7} - \frac{1}{r}\right)\left(\frac{r_0}{r}\right)^6 \tag{9}$$

However, it is worth noting that the 6–12 potential is only a special calibration form of the Lennard-Jones potential. The calibration of the powers of the gravitational and repulsive terms is based on the microscopic particles in the fluid and the interaction between them. In the scene of the car-following behavior, the magnitude of the two interacting objects is quite different from that of the particles in terms of mass, speed or acceleration. Therefore, simply applying the 6–12 potential to the actual car-following behavior will make the current vehicle extremely sensitive to changes in the speed and distance of the preceding vehicle. To solve this problem, we set the power v and u of the gravitational and repulsive terms as the parameters to be calibrated in the model, and construct the function for vehicle potential field as follows:

$$U_{\mathrm{V}} = \frac{\varepsilon}{v-u}\left[u\left(\frac{X_{\mathrm{r}}}{L}\right)^v - v\left(\frac{X_{\mathrm{r}}}{L}\right)^u\right] \tag{10}$$

The derivative function of the interacting potential between vehicles to displacement is as follows:

$$f_{\mathrm{v}} = \frac{vu\cdot\varepsilon}{v-u}\left(\frac{X_{\mathrm{r}}^u}{L^{u+1}} - \frac{X_{\mathrm{r}}^v}{L^{v+1}}\right) \tag{11}$$

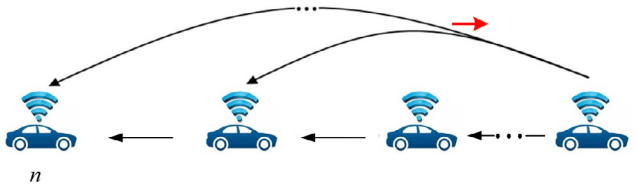

Fig. 6. Schematic diagram of car-following scene of CAVs.

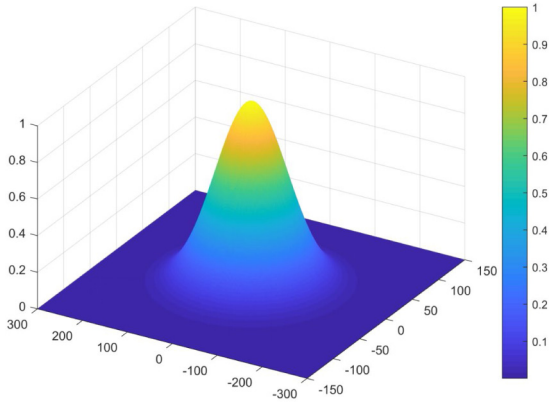

Fig. 7. The distribution of potential field generated by one vehicle.

We assume the mass of the vehicle is M and let $\eta_1 = \frac{vu \cdot \varepsilon}{M(v-u)}$ to simplify model. Then the expression of the car-following acceleration generated by the vehicle potential field is as follows:

$$a = \eta_1 \left(\frac{X_r^u}{L^{u+1}} - \frac{X_r^v}{L^{v+1}} \right) \tag{12}$$

It can be seen from the expression that this potential field only considers the effect of the distance between adjacent preceding and current vehicles and the relative speed. It is more suitable for traditional traffic. For the intelligent and connected environment, CAV can also obtain the information of acceleration of the preceding vehicle in real time based on communication and sensing technology, as shown in Fig. 6. In view of this, the acceleration of the preceding vehicle is introduced into the required safe distance of the following vehicle, which can be expressed as follows:

$$X_r' = (t_0 - c_v v_r - c_a \dot{v}_{n+1})\, v_n \tag{13}$$

where $\dot{v}_{n+1}$ is the acceleration of the preceding vehicle, and t_0, c_v, and c_a are coefficients to be calibrated and greater than zero.

Generally speaking, on the potential field plane, the strength of the potential field at any point is related to the distance of the target vehicle. Within the required safe distance range, the intensity increases as the distance decreases, and reaches the maximum value at the target vehicle's position, as shown in Fig. 7. We assume that the spatial coordinate position of vehicle's centroid is (x_0, y_0). Without taking into account lane-changing behavior, the distance d from any point in space to the centroid can be expressed as follows:

$$d = \sqrt{(x - x_0)^2 + (y - y_0)^2} \tag{14}$$

Different running states of vehicles will have different effects on the distribution of the potential field. In addition to the relative position between the vehicles, the current vehicle's speed and acceleration are also the main factors affecting the distribution of the potential field. On the other hand, considering that there is almost no component of speed in the lateral direction of vehicle in the simple scenario of a single lane, and the change of vehicle's speed does not significantly change the safe risk. Based on the above analysis, the modified short-range repulsive distributed range of potential field can be expressed as follows:

$$|d'| = \sqrt{s_0 (x - x_0)^2 + \left[\frac{s_0}{e^{\gamma X_r'}} (y - y_0) \right]^2} \tag{15}$$

In the equation, the traveling direction of the vehicle is the y-axis, the vertical to the traveling direction of the vehicle is the x-axis, and γ is the undetermined coefficient, s_0 is the minimum safe distance for braking.

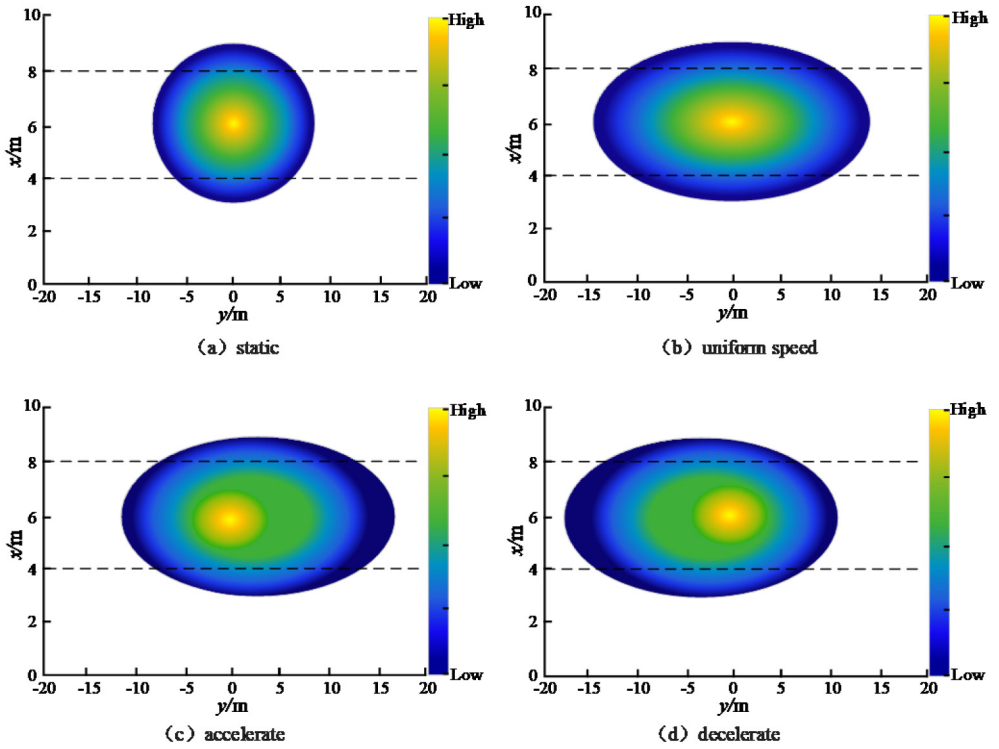

Fig. 8. Short-range repulsive potential field distribution of the vehicle under different driving states.

Therefore, this paper constructs a vehicle potential field model considering the parameters of the vehicle's motional state as follows:

$$U_V = \frac{\frac{\varepsilon}{v-u}\left[u\left(\frac{X_r'}{L}\right)^v - v\left(\frac{X_r'}{L}\right)^u\right]\cdot e^{\sin\theta}}{|d'|}\cdot\frac{d'}{|d'|} \tag{16}$$

where θ is the clockwise angle formed from any point around the target vehicle to the center of the vehicle and the direction of vehicle's movement.

The followings are to analyze the characteristics of the potential field of the vehicle through contour projection of the potential field within the required safe distance, as shown in Fig. 8.

(1) When the target vehicle is at a standstill, as shown in Fig. 8(a), the contour projection of the potential field in this scene consists of several concentric circles, which means that within the same distance, regardless of the angle of another vehicle approaching the target vehicle has the same safe risk. In this case, the vehicle can be regarded as an obstacle.

(2) When the target vehicle moves along the y-axis (vehicle's direction) at a constant speed $v = 20$ m/s, as shown in Fig. 8(b). Compared with Fig. 8(a), no matter how the vehicle's speed changes in the y-axis direction (across the lanes), its strength of potential field and repulsive range in the x-axis direction remain unchanged, because the component of vehicle's speed in the x-axis direction remains unchanged. On the contrary, the vehicle's short-range repulsive range increases with the increase of the target vehicle's speed in the y-axis direction, and the potential field's strength decreases symmetrically along the gradient of the vehicle's front and rear directions. In this case, the contour projection of the vehicle potential consists of several concentric ellipses.

(3) When the target vehicle accelerates and decelerates along the y-axis with an acceleration of 1 m/s^2, as shown in Fig. 8(c) and (d) respectively. In these two cases, even if the speed of the vehicle at this time is consistent with Fig. 8(b), the range of short-range repulsion and the distribution of the potential field are significantly different from those in the uniform state. The distribution under this situation is obviously inclined to the front or the rear.

3. Car-following model with safe potential field

Through the above analysis, it is concluded that the safe potential field U composed of the lane marking potential field U_L, the road boundary potential field U_R and the vehicle potential field U_V can dynamically describe the CAV's safe risks

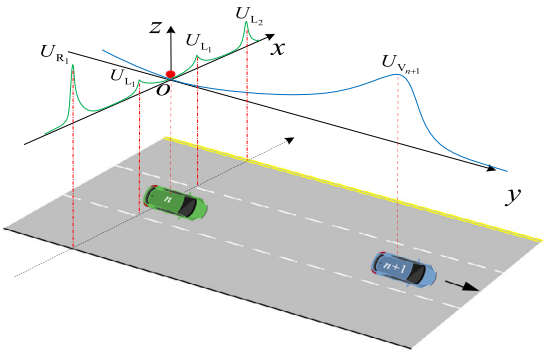

Fig. 9. The diagrammatic sketch of car following under safe field.

during the driving process, and the final mode of vehicle safe potential field can be expressed as follows:

$$U = U_{\mathrm{L}} + U_{\mathrm{R}} + U_{\mathrm{V}} \tag{17}$$

The vehicle can determine its microscopic motional behavior according to the total potential field distribution of its surrounding traffic environment. The microscopic behavior of the vehicle mainly includes two aspects, car following and lane changing. For the moment, CAV still has to ensure the safety as the primary condition, that is, CAV will try its best to seek the lower point of the total potential field under the constraints of various potential fields, as shown in Fig. 9. The center of the vehicle is shown with a red ball.

Since the vehicle's following behavior can be regarded as a motion under various forces, the resultant force of the following vehicle can be obtained by derivative of U to displacement, and then the car-following model based on the safe potential field (SPF) can be obtained as follows:

$$\dot{v}_n = \frac{\dfrac{\partial U_{\mathrm{L}}}{\partial x} + \dfrac{\partial U_{\mathrm{R}}}{\partial x} + \dfrac{\partial U_{\mathrm{V}}}{\partial y}}{\mathrm{M}} \tag{18}$$

4. Calibrate model's parameters

4.1. Data preparation

The acceleration information of the vehicle is no longer simply detected by the on-board equipment, but obtained by vehicle–vehicle wireless communication technology. However, at present, most of the intelligent vehicles operate independently, and the intelligent and connected environment is not yet available. In the traditional environment, although the driver cannot obtain the specific value of the motional information of the preceding vehicle, but can basically respond to the speed change of the preceding vehicle in a timely manner. Therefore, the Shanghai Natural Driving Data Set [40], which is more in line with the driving habits of Chinese people, is selected. The project collected driving behavior data of more than 60 people and a cumulative mileage of more than 160,000 km. The project uses SHRP2 NextGen data acquisition system to connect the tested vehicle and the three-axis accelerometer, camera, radar and GPS installed to obtain high-precision data information of vehicle operation. The sampling frequency of the system is distributed from 10 to 50 Hz. According to the process of data extraction shown in Fig. 10, the following rules are formulated: ① Determine the value of D to ensure that the preceding vehicle is in the radar range of the tested vehicle; ② Judge the value of longitudinal spacing headway S to eliminate the data of the tested vehicle in a free flow; ③ Judge the value of car-following duration T to ensure the minimum time the vehicle lasts in a car-following segment, and the purpose is to extract vehicle's operating data under multiple speed changes. Based on the above rules, 1600 car-following segments of 30 drivers were extracted. After manual comparison, 1560 effective segments were finally extracted, of which 1040 and 520 segments were randomly selected as the calibration set and the verification set, respectively. Table 1 shows 140 random car-following segments.

4.2. The choice of algorithm

There are many algorithms for calibrating parameters, including Newton down-hill method, ant colony optimization and genetic algorithm. Due to the high robustness of genetic algorithm, it can be solved quickly under the condition of multi parameters, and it is not easy to fall into the local optimum, so we use this algorithm for calibration, and its main execution process is shown in Fig. 11.

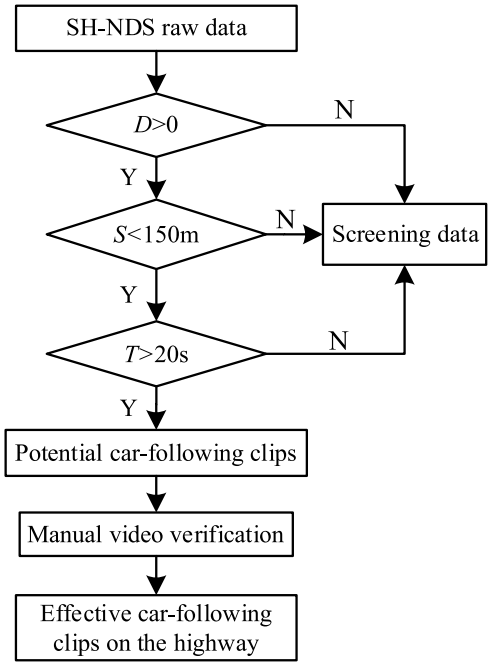

Fig. 10. The extractive process of effective car following segment.

Table 1
Random samples and related parameters of car following segments.

Car-following clips	Duration (s)	Vehicles' speed (km/h)		Longitudinal relative speed (m/s)		Spacing Headway (m)	
		Minimum	Maximum	Minimum	Maximum	Minimum	Maximum
1	47.34	82	108	−2.71	2.06	27.37	81.43
2	162.45	112	120	−1.32	0.71	39.74	103.81
3	47.12	92	115	−2.46	1.27	21.51	85.77
4	154.74	101	118	−1.05	0.93	32.57	111.28
5	20.71	89	117	−2.59	1.82	15.39	102.54
6	167.48	112	118	−0.75	0.55	45.22	95.89
7	27.94	109	114	−0.88	1.02	58.48	92.36
⋮							
137	31.49	83	97	−1.31	1.22	9.45	62.15
138	24.78	97	115	−2.13	1.49	17.54	86.24
139	274.55	117	120	−0.15	0.21	24.78	109.58
140	51.31	93	103	−1.68	0.85	11.49	78.69

We select vehicle's speed and space headway to calibrate the parameters of the model, and use Root Mean Square Percentage Errors (RMSPE) as the objective function to measure the deviation between the measured value and the simulated value. The expression is as follows:

$$R_{\mathrm{RMSPE}} = \sqrt{\frac{\sum_{i=1}^{N}\left(V_i^{\mathrm{s}} - V_i^{\mathrm{r}}\right)^2}{\sum_{i=1}^{N}\left(V_i^{\mathrm{r}}\right)^2}} + \sqrt{\frac{\sum_{i=1}^{N}\left(S_i^{\mathrm{s}} - S_i^{\mathrm{r}}\right)^2}{\sum_{i=1}^{N}\left(S_i^{\mathrm{r}}\right)^2}} \tag{19}$$

where N is the total number of samples, i is the serial number of the sample, V_i^{s} and V_i^{r} are the simulated speed and real speed of the ith sample respectively, S_i^{s} and S_i^{r} are the simulated and real space headway of the ith sample respectively.

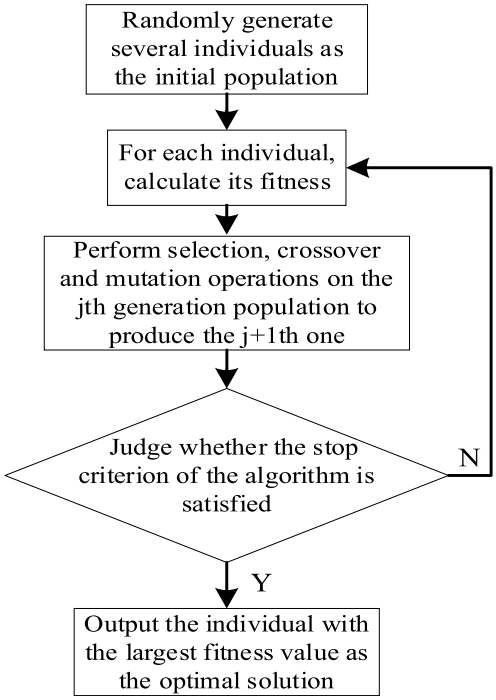

Fig. 11. The process of genetic algorithm.

Table 2
Calibrated results of the parameters in the model.

parameters	values
u	0.713
v	1.648
η_0	28.535
η_1	43.531
γ	0.032
s_0	2.11

4.3. Results of calibration

We use the genetic algorithm toolbox in Matlab to solve algorithm. The population size is set to 400, the maximum genetic algebra is set to 300, the cut-off algebra is set to 100, the allowable error of convergence is set to 10^{-6}, each calibration is repeated 5 times, and the one with the smallest error is taken as the result of parameter calibration, as shown in Table 2.

5. Effect evaluation of the model

In order to evaluate the effect of the model built in this article, we chose to compare with IDM and VTH models. The reason is that IDM contains parameters which reflect the time headway between vehicles, while VTH is a kind of car-following strategy with variable time headway. The time headway under this strategy is not only related to the speed of the current vehicle but also to the speed of the preceding vehicle.

The IDM model is as follows:

$$\dot{v}_n = a_{\max}[1 - \left(\frac{v_n}{v_d}\right)^{\beta} - \left(\frac{s_0 + v_n t_d - \frac{v_n \cdot v_r}{2\sqrt{a_{\max} \cdot a_{com}}}}{L}\right)^2] \tag{20}$$

where $\dot{v}_n$ is the acceleration of the nth vehicle, $a_{\max}$ is the maximum acceleration of the vehicle, v_n is the instantaneous speed of the nth vehicle, v_d is the driver's desired speed, β is the power series of velocity; L is real-time space headway; t_d is the time headway; s_0 is minimum safe braking distance, v_r is the relative speed; a_{com} is the comfortable deceleration.

Table 3
Result of parameter calibration of IDM and VTH model.

parameters	values
$a_{\max}$	1.42 m/s^2
a_{com}	1.68 m/s^2
v_{d}	33.33 m/s
s_0	2.11 m
T_n	1.52 s
β	4.00
t_0	1.5 s
c_v	0.05

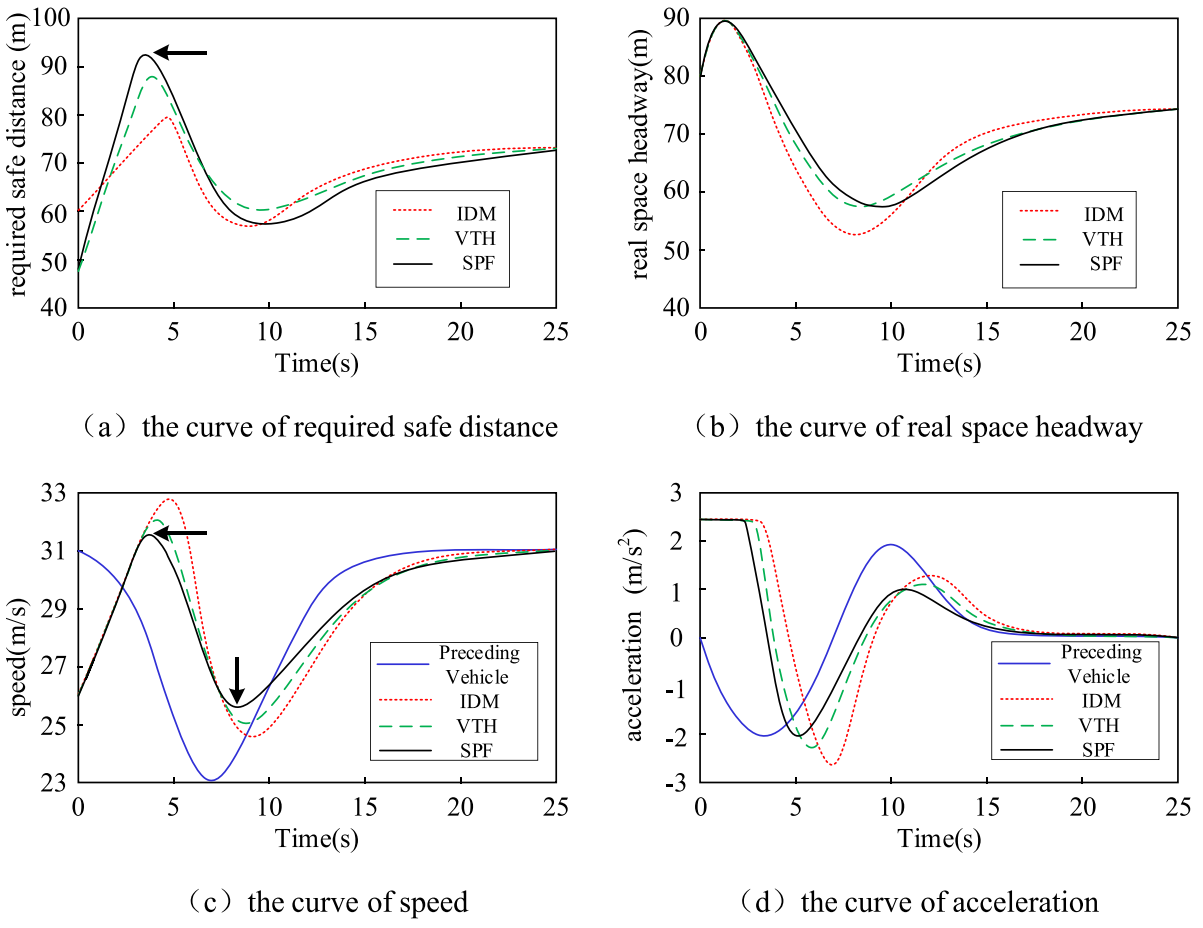

Fig. 12. Response curves of different models in the scene of frequent speed changes of preceding vehicle.

The VTH model is as follows:

$$t_{\text{d}} = t_0 - c_v v_{\text{r}} \tag{21}$$

where t_d is the value of the time headway; t_0 and c_v are the coefficients to be calibrated; v_{r} is the relative speed with the preceding vehicle.

We use the same data set and algorithm to calibrate the parameters of IDM and VTH models, the results are shown in Table 3.

In order to effectively evaluate the performance of the three models under different conditions of the vehicle, we select the typical scenarios of frequent speed changes of the preceding vehicle, long-distance approaching to the preceding vehicle, and sudden braking of the preceding vehicle for simulation, and we compare and analyze the response characteristic of following vehicle under different traffic conditions to verify the validity of the built model.

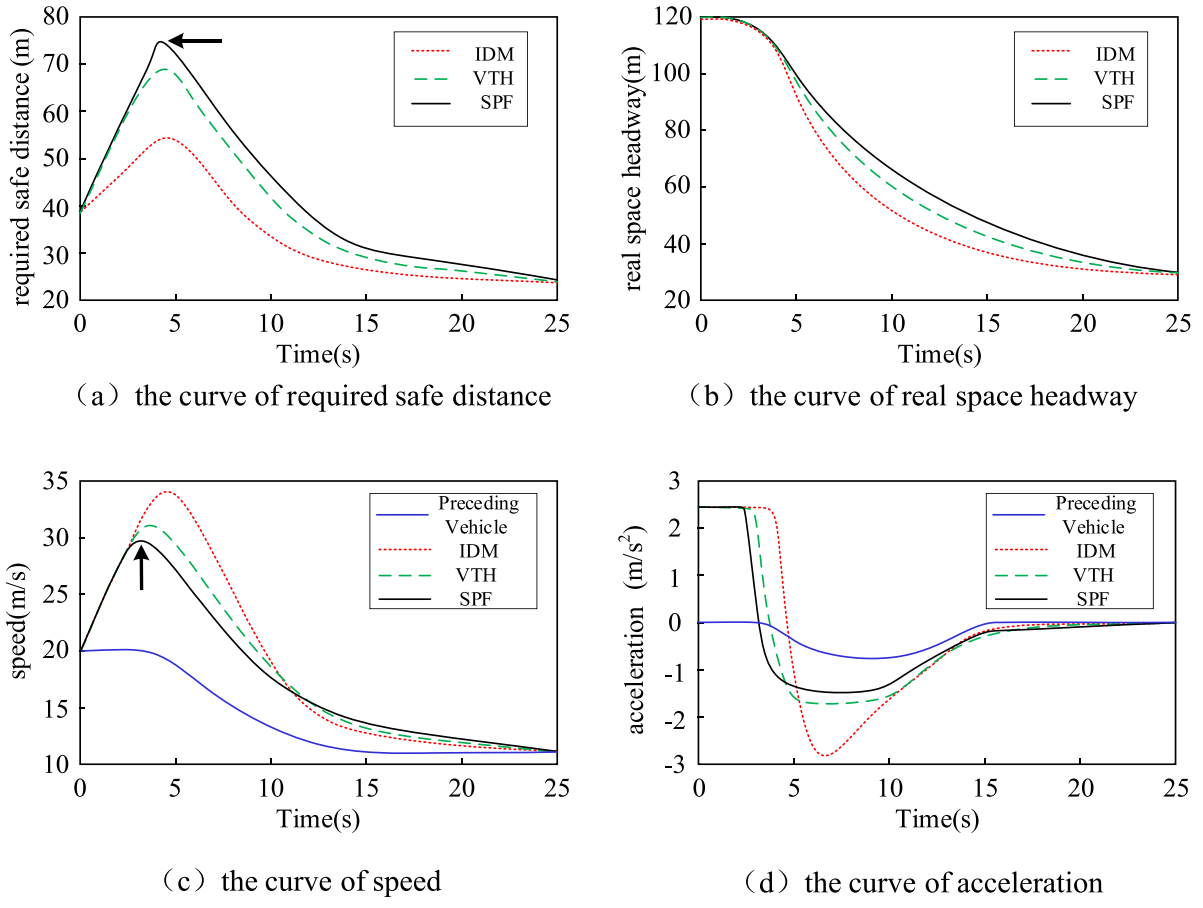

Fig. 13. Response curves of different models in the scene of long distance car following.

(1) In the scene of frequent speed change of the preceding vehicle, the simulated initial time headway is set to 80 m, and the initial speeds of the front and current vehicles are 31 m/s and 26 m/s respectively. The whole process makes the preceding vehicle accelerate and decelerate to a certain extent. The response curves of the following vehicle obtained under different models are shown in Fig. 12.

It can be seen from the results that in the three models, the following vehicle accelerates correspondingly in the initial stage to catch up with the preceding one, but with the deceleration of the preceding vehicle, the following vehicle has to decelerate to adapt to the preceding vehicle, as shown in Fig. 12(a). Because the acceleration of the vehicle in front is considered in SPF model, when the acceleration of the preceding vehicle is negative, the required safe distance of SPF model is larger than that of IDM and VTH models, and it decelerates first at 3.6 s to avoid collision with the preceding vehicle. Under the IDM and VTH models, the following vehicle starts to decelerate at 5 s and 4 s, respectively, as shown in Fig. 12(c). In addition, the lag of deceleration response can be seen from the maximum deceleration in Fig. 12(d) and it will cause more severe deceleration in the future. As time goes by, when $t = 7$ s, the vehicle in front starts to accelerate, and the threat from the rear vehicle decreases. At the same time, under the SF model, when the following vehicle obtains the acceleration of the preceding vehicle as positive, its required safe distance will be appropriately reduced under the premise of ensuring safety, and it will accelerate first at 8.4 s, while under IDM and VTH models, the following vehicle gradually starts to accelerate at 9.3 s and 8.8 s respectively, and the lag of the acceleration response also occurs, which makes the subsequent accelerated phenomenon more severe. To sum up, in the conventional car-following scene, the SPF model has better adaptability and predictability. It can better ensure the safety of the following vehicle by increasing the required safe distance when the preceding vehicle is decelerating, and reducing the required safe distance to improve the efficiency when the preceding vehicle is accelerating.

(2) In the scene of approaching the preceding vehicle at a long distance, the initial speed of the front and current vehicle are set to 20 m/s, and the initial space headway is set to 120 m. In the whole process, the preceding vehicle is driven at a uniform speed first and then decelerated. The response curves of the following vehicle under different models are obtained, as shown in Fig. 13.

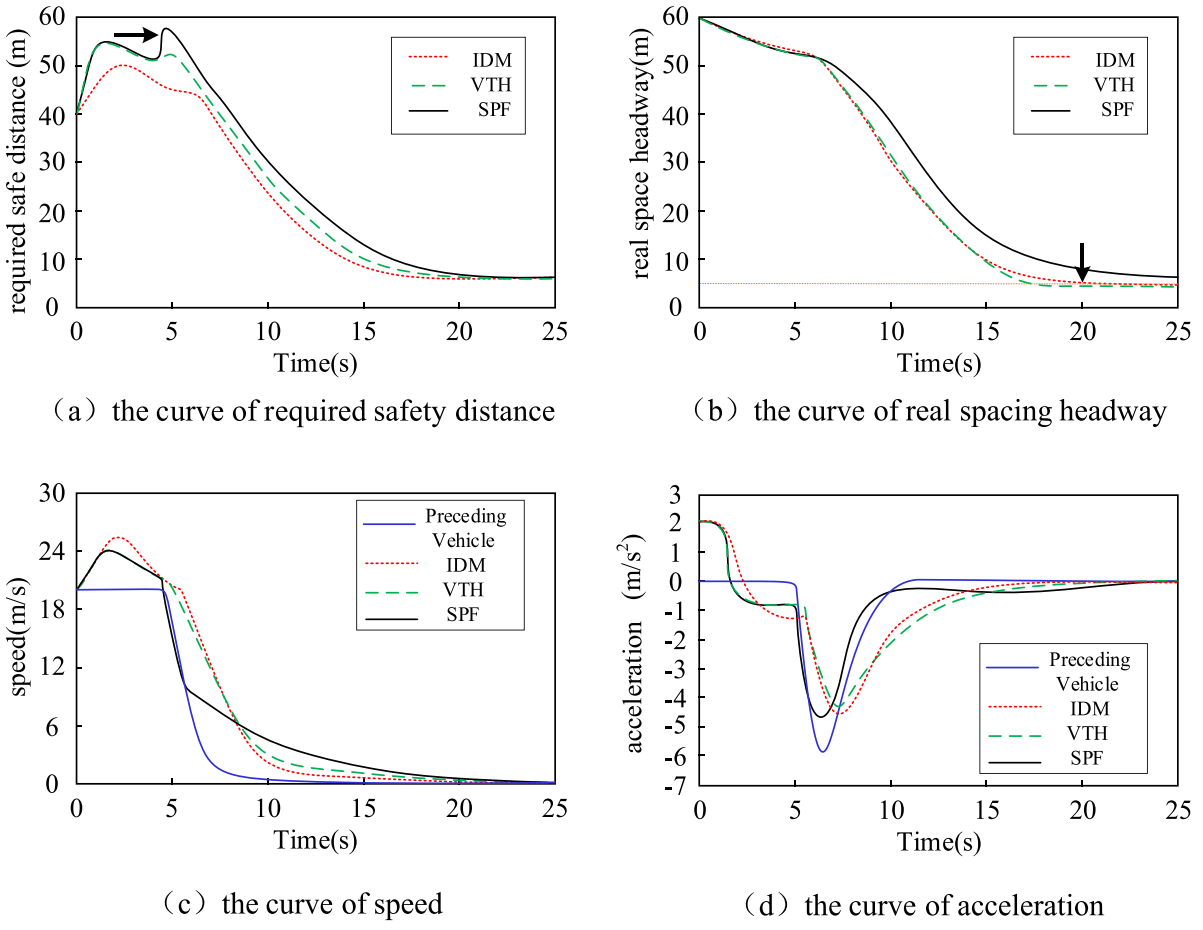

Fig. 14. Response curves of different models in the scene of preceding vehicle emergency braking.

The results show that the following vehicle in SPF model is attracted by the preceding vehicle at the initial stage. Like the other two models, the following vehicle in SPF model takes a larger acceleration to approach the preceding one, and the required safe distance increases with the increase of speed. However, when the preceding vehicle begins to decelerate, the following vehicle under SPF model can obtain the changing information in time, and its required safe distance becomes larger, which makes the long-distance attraction of the preceding vehicle quickly become short-range repulsion, and decelerates at 3.2 s first. However, IDM and VTH models cannot accurately perceive this change, and the following vehicle begins to decelerate at 4.5 s and 3.7 s respectively, as shown in Fig. 13(c). The lag of response leads to the subsequent change of speed (i.e. acceleration) becoming more intense, as shown in Fig. 13(d). In the whole approaching process, it can be seen that SF model can respond to the speed change of the preceding vehicle in time, which makes the following vehicle's speed change more smoothly and improves the driving safety.

(3) The scene of preceding vehicle braking can test the driving safety of the model to the greatest extent. The initial speeds of the front and current vehicles are set as 20 m/s, and the initial space headway is set as 60 m. When $t = 5$ s, the preceding vehicle will brake sharply, and the speed will decrease to zero rapidly. The response curves of each model in this case are shown in Fig. 14.

From the results, it can be seen that the preceding vehicle braked suddenly at 5 s, and the safe potential field formed by the short-range repulsion in the backward direction rapidly increased. Due to considering the acceleration of the preceding vehicle, the following vehicle in SPF model can obtain the information of acceleration changing at 5 s. It increases its own required safe distance and brakes in time, so as to avoid collision with the vehicle in front. The following vehicle under IDM and VTH models both collided with the preceding vehicle after 20 s (the real space headway < vehicle length i.e. 5 m), as shown in Fig. 14(b), which proves that SPF model can effectively improve the safety of the following vehicle in this scenario.

6. Conclusion

(1) We apply the potential field theory to the traffic system in the intelligent and connected environment, and the established model can intuitively describe the influence of traffic factors on CAV through the potential field formed by various factors. The model also can reflect the degree of safe risk in the driving process through the strength of potential field, which can lay the foundation for the safe decision of CAV.
(2) In order to make up for the defects that the existing function of vehicle potential field is independent, we establish the function of vehicle potential field based on Lennard-Jones to describe the behavior between vehicles, so as to smooth the transition between gravitation and repulsion. It makes the vehicle potential field more reasonable and unified.
(3) We introduce acceleration into the safe potential field model and apply it to the car-following behavior of CAV. The simulation results prove that, compared with the classical IDM and VTH models, the following vehicle in this model performs better under the condition of frequent oscillation of the speed of the vehicle in front. Even when the speed of preceding vehicle changes sharply (i.e. sudden braking), it still has a smoother response curve to avoid collision and improve the driving safety and efficiency, which proves that this model has better predictability and stability.
(4) At present, the safe potential field and car-following model established in this paper are only limited to simple highway scenarios. In the future, CAVs will be gradually popularized in urban roads. At that time, the traffic environment will also include non-motor vehicles and pedestrians besides the factors considered in this paper. The environment will become more complex, and the safe requirements for CAVs will be higher, this is also the research direction that needs to be focused next.

Funding

This study was funded by the National Natural Science Foundation of China (Grant no. 51678320) and Key R&D Plan of Shandong Province (Grant no. 2019GGX101038). All authors approved the version of the manuscript to be published.

CRediT authorship contribution statement

Yanfeng Jia: Wrote the paper, Conceived and designed the research. **Dayi Qu:** Conceived and designed the research. **Hui Song:** Performed the experiments. **Tao Wang:** Analyzed the data. **Zixu Zhao:** Analyzed the data.

Declaration of competing interest

The authors declare that they have no known competing financial interests or personal relationships that could have appeared to influence the work reported in this paper.

References

[1] P.G. Gipps, A behavioural car-following model for computer simulation, Transp. Res. B 15 (1981) 105–111.
[2] R. Jiang, Q.S. Wu, Z.J. Zhu, A new continuum model for traffic flow and numerical tests, Transp. Res. B 36 (2002) 405–419.
[3] H. Ou, T.Q. Tang, Impacts of moving bottlenecks on traffic flow, Physica A 500 (2018) 131–138.
[4] S.W. Yu, X.M. Zhao, Z.G. Xu, L.C. Zhang, The effects of velocity difference changes with memory on the dynamics characteristics and fuel economy of traffic flow, Physica A 461 (2016) 613–628.
[5] G.J. Andersen, C.W. Sauer, Optical information for car following: The driving by visual angle (DVA) model, Hum. Factors 49 (2007) 878–896.
[6] W. Van Winsum, The human element in car following models, Transp. Res. F 2 (1999) 207–211.
[7] Y.Q. Sun, H.X. Ge, R.J. Cheng, An extended car-following model considering driver's memory and average speed of preceding vehicles with control strategy, Physica A 521 (2019) 752–761.
[8] D.C. Gazis, H. Rothery, Nonlinear follow-the-leader models of traffic flow, Oper. Res. 9 (1961) 545–567.
[9] G.F. Newell, Nonlinear effects in the dynamics of car following, Oper. Res. 9 (1961) 209–229.
[10] G.H. Peng, R.J. Cheng, A new car-following model with the consideration of anticipation optimal velocity, Physica A 392 (2013) 3563–3569.
[11] Q. Sun, Z.Y. Guo, Vehicle following model based on long short-term memory neural network, J. Jilin U.: Techno. Ed. 50 (2020) 1380–1386.
[12] B. Zhu, Y.D. Jiang, J. Zhao, H. Chen, W.W. Deng, A car-following control algorithm based on deed reinforcement learning, China J. High. Transp. 32 (2019) 53–60.
[13] X. Zhao, Z. Gao, A new car-following model: full velocity and acceleration difference model, Eur. Phys. J. B. 47 (2005) 145–150.
[14] G.H. Peng, D.H. Sun, A dynamical model of car-following with the consideration of the multiple information of preceding cars, Phys. Lett. A 374 (2010) 1694–1698.
[15] W. Pan, Y. Xue, H.D. He, et al., Impacts of traffic congestion on fuel rate, dissipation and particle emission in a single lane based on nasch model, Physica A 503 (2018) 154–162.
[16] Y. Chen, W. Zhang, Dynamic model of high speed following traffic flow, Acta Phys. Sin. Chin. Ed. 69 (2020) 136–148.
[17] M. Treiber, A. Hennecke, D. Helbing, Congested traffic states in empirical observations and microscopic simulations, Phys. Rev. E 62 (2000) 1805–1824.
[18] O. Khatib, Real-time obstacle avoidance system for manipulators and mobile robots, Ind. Robot. 5 (1986) 90–98.
[19] T. Sattel, T. Brandt, From robotics to automotive: Lane-keeping and collision avoidance based on elastic bands, Veh. Syst. Dyn. 46 (2008) 597–619.
[20] D. Ni, A unified perspective on traffic flow theory. Part I: The field theory, Appl. Math. Sci. 7 (2013) 1929–1946.

[21] T.P. Hsu, G.Y. Weng, Y.J. Lin, Conceptual structure of a novel car-following model upon gravitational field concept, in: 19th ITS World Congress, 2012.
[22] M.T. Wolf, J.W. Burdick, Artificial potential functions for highway driving with collision avoidance, in: IEEE International Conference on Robotics & Automation, 2008.
[23] J. Wang, J. Wu, Y. Li, The driving safety field based on driver–vehicle–road interactions, IEEE Trans. Intell. Transp. 16 (2015) 2203–2214.
[24] D.Y. Qu, J. Li, C. Liu, D.M. Liu, Y.F. Jia, Dynamic characteristics model of traffic flow based on molecular dynamics, J. Transp. Syst. Eng. Inf. Technol. 17 (2017) 188–194.
[25] C. Li, X. Jiang, W. Wang, et al., A simplified car-following model based on the artificial potential field, Procedia Eng. 137 (2016) 13–20.
[26] Z.S. Yang, Y. Yu, D.X. Yu, et al., APF-based car following behavior considering lateral distance, Adv. Mech. Eng. 2013 (2013) 1255–1260.
[27] W. Liu, Z. Li, Comprehensive predictive control method for automated vehicles in dynamic traffic circumstances, IET Intell. Transp. Syst. 12 (2018) 1455–1463.
[28] L. Li, J. Gan, Z. Yi, et al., Risk perception and the warning strategy based on safety potential field theory, Accident Anal. Prev. 148 (2020) 105805, http://dx.doi.org/10.1016/j.aap.2020.105805.
[29] L. Li, J. Gan, Z. Yi, et al., Dynamic driving risk potential field model under the connected and automated vehicles environment and its application in car-following modeling, IEEE Trans. Intell. Transp. (2020) http://dx.doi.org/10.1109/TITS.2020.3008284.
[30] L. Li, J. Gan, Z. Yi, et al., A dynamic control method for Cavs Platoon based on the MPC framework and safety potential field model, KSCE J. Civ. Eng. 25 (2021) 1874–1886.
[31] X. Hua, W. Wang, H. Wang, A car-following model with the consideration of vehicle-to-vehicle communication technology, Acta Phys. Sin. Chin. Ed. 65 (2016) 13–25.
[32] B. Wu, W. Wang, L. Li, Y. Liu, Longitudinal control model for connected autonomous vehicles influenced by multiple preceding vehicles, J. Traff. Transp. Eng. 20 (2020) 184–194.
[33] Y. Qin, H. Wang, W. Wang, D. Ni, Review of car-following models of adaptive cruise control, J. Traff. Transp. Eng. 17 (2017) 121–130.
[34] B. Gunay, Methods to quantify the discipline of lane-based-driving, Traff. Eng. Cont. 44 (2003) 22–27.
[35] M.T. Wolf, J.W. Burdick, Artificial potential functions for highway driving with collision avoidance, in: IEEE International Conference on Robotics & Automation, Pasadena, CA, 2008, pp. 19–23.
[36] L. Li, J. Gan, K. Zhou, X. Qu, B. Ran, A novel lane-changing model of connected and automated vehicles: Using the safety potential field theory, Physica A 559 (2020) 125039.
[37] Y. Jia, D. Qu, L. Han, et al., Research on car-following model based on molecular dynamics, Adv. Mech. Eng. 13 (2021) 168781402199300.
[38] D. Yanakiev, I. Kanellakopoulos, Nonlinear spacing policies for automated heavy-duty vehicles, IEEE Trans. Veh. Technol. 47 (1998) 1365–1377.
[39] D.M. Ferguson, P.A. Kollman, Can the Lennard–Jones 6-12 function replace the 10-12 form in molecular mechanics calculations? J. Comput. Chem. 12 (1991) 620–626.
[40] X.S. Wang, M.X. Zhu, Y.L. Xing, Impacts of collision warning system on car-following behavior based on naturalistic driving data, J. Tongji Univ. Nat. Sci. Ed. 44 (2016) 1045–1051.